Nuclear Instruments and Methods in Physics Research A 397 (1997) 448–454

NUCLEAR INSTRUMENTS & METHODS IN PHYSICS RESEARCH Section A

ELSEVIER

Integrated measurements of ^{218}Po, ^{214}Pb and ^{214}Bi + ^{214}Po in air under environmental concentrations

Dobromir S. Pressyanov

Department of Atomic Physics, St. Kliment Ohridski University of Sofia, 5 James Bourchier Blvd., Sofia-1164, Bulgaria

Received 12 August 1996; received in revised form 18 February 1997

Abstract

A method determining time-integrated concentrations of each of the short-lived ^{222}Rn progeny (^{218}Po, ^{214}Pb and ^{214}Bi + ^{214}Po) in air is proposed. It is based on the combination of an aerosol filter rotating with a period of 1 h and LR-115 type II solid state nuclear track detectors shielded with absorbers. The method is intended to work at integrated concentrations as low as 100 Bq h m^{-3} and to enable quantitative measurements in a mixed ^{222}Rn and ^{220}Rn atmosphere. If ^{220}Rn progeny are present in measurable concentrations, their potential alpha energy concentration (PAEC) could be estimated as well. Experimental tests have been performed in the range of ^{222}Rn progeny integrated concentrations of 20–5000 Bq h m^{-3} and for ^{218}Po : ^{214}Pb : ^{214}Bi activity ratios ranging from a substantial disequilibrium (1 : 0.3 : 0.1) to about an equilibrium state. The experimental results presented suggest that the sensitivity of the method is sufficient for integrated measurements indoors and outdoors.

Keywords: ^{222}Rn progeny; Radon; Integrated measurements; Environment

1. Introduction

At present ^{222}Rn is believed to contribute about half of the effective dose from natural sources. The organ at major risk is the lung and as found in Ref. [1] the lung dose is delivered almost entirely by the short-lived ^{222}Rn progeny (i.e. ^{218}Po, ^{214}Pb and ^{214}Bi + ^{214}Po; ^{214}Po is always in equilibrium with ^{214}Bi). Large projects for screening of radon indoors have been conducted in a number of countries [2]. Most of these projects are based on integrated measurements of ^{222}Rn-gas alone by a number of techniques [3]. These measurements are simple and cost-efficient. However, the knowledge of the individual concentrations of each of the radionuclides ^{218}Po, ^{214}Pb and ^{214}Bi is important for: dose assessment and in research on the behavior and removal of ^{222}Rn progeny under different conditions, study of the effect of ventilation and other methods of mitigation, etc. A number of grab-sampling methods for instantaneous ^{222}Rn-progeny measurements are described in the literature [4–8]. The measured concentrations are not representative for intervals much longer than the time of grab-sampling (few minutes) because of the large time variations of ^{222}Rn-progeny concentrations in air.

An experimental approach for integrated measurements of ^{218}Po, ^{214}Pb and ^{214}Bi + ^{214}Po in air has been proposed in Ref. [9]. The idea is based on the uniformly rotating filter. Each point of the filter passes through the inlet nozzle and the detectors placed above the filter (Fig. 1(a)). Due to the radioactive decay of the radionuclides deposited on the filter, their surface specific activities and hence, the signal of the detectors depend on the angular position. Conceptually, a similar approach has been used for measuring radon progeny deposited on surfaces [10]. Thermoluminescence detectors (TLDs) have been initially used for experiments under high concentrations of ^{222}Rn progeny (uranium mines and radon spas) [11]. However, at present a great concern are ^{222}Rn and ^{222}Rn-progeny measurements in dwellings [2,12] and in some cases outdoors [13–15]. The concentrations under these conditions are usually much lower and the TLDs-based version lacks the required sensitivity in this range of interest [16].

In the present work we propose a method of integrated measurements of ^{218}Po, ^{214}Pb and ^{214}Bi that is based on a combination of a filter uniformly rotating at velocity of one revolution per hour and solid-state nuclear track detectors (SSNTDs). This arrangement allows individual integrated concentrations of each of the ^{222}Rn progeny to be quantitatively estimated at levels typical for indoor and outdoor air. The method accounts for the presence of ^{220}Rn progeny (i.e. ^{212}Pb and ^{212}Bi + ^{212}Po) in a mixed ^{222}Rn and ^{220}Rn atmosphere. Comparative measurements have been made using series of grab-sampling

PII S0168-9002(97)00769-9

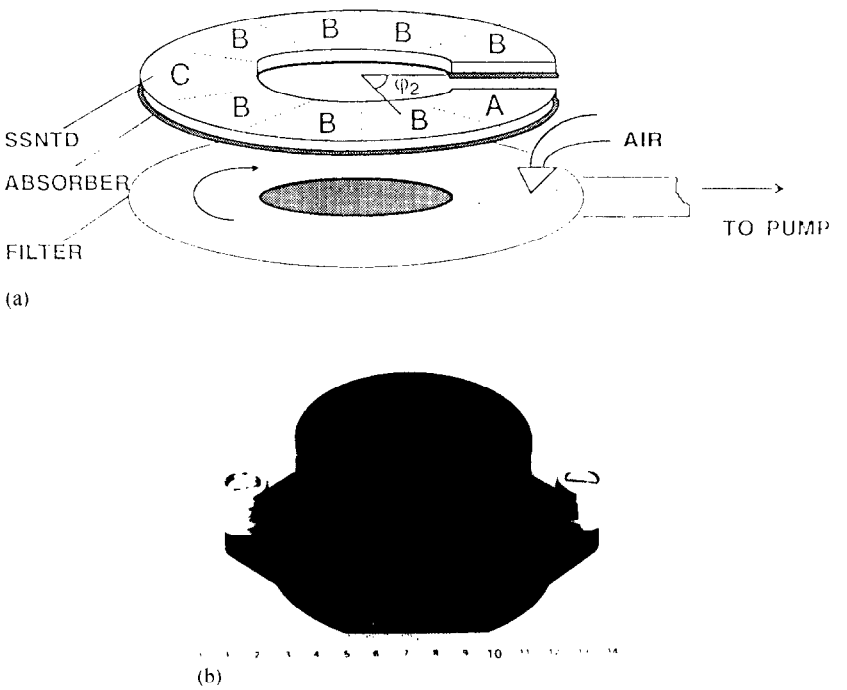

Fig. 1. (a) A principal scheme of the experimental device with a configuration of different sectors. The angles φ_k of the sector centers (φ_2 illustrated) are measured from the start position of the inlet nozzle (i.e. $\varphi = 0^\circ$ for a point which enters the inlet nozzle area). In the real device the distance between the filter and the absorber + SSNTD is less than 1 mm. (b) A photo of the experimental device. The scale is in cm.

measurements as a reference. The experimental results suggest that the method is sensitive at integrated concentrations as low as 100 Bq h m^{-3} suitable for measurements indoors and outdoors.

2. Experimental

The principal scheme of the experimental device is shown in Fig. 1(a), and the photo of the instrument in Fig. 1(b). The filter is moved by a battery-supplied electric clock mechanism. The whole device is mounted inside a metal housing, where the air enters through ten $\varnothing$ 2 mm holes situated above the inlet nozzle as shown in Fig. 1(b). In the present arrangement "detectors" are different sectors of the Kodak–Pathe LR-115 type II film formed as shown in Fig. 1(a). The sectors are shielded with absorbers that reduce the energies of the α-particles (6.0 MeV for ^{218}Po and 7.69 MeV for ^{214}Po) to the range of sensitivity of this type of detectors. Etched tracks in LR-115 II detectors can be observed only if the energies of the α-particles are within the energy window and their incident angle (to the normal of the detector's surface) is less than a "critical angle". Both upper and lower limits of the energy window and the critical angle may vary depending on the etching procedure and the manner of track counting. The values used as a reference (for orientation only) in the present work are 1.5–4.5 MeV for the energy window and $\theta_c \leq 60^\circ$ for the critical angle [17].

Theoretically calculated dependencies of the surface specific activity of α-active ^{222}Rn progeny: ^{218}Po and ^{214}Po (i.e. ^{214}Bi + ^{214}Po) on the angular position φ (Fig. 1(a)) are shown in Fig. 2. The curves in Fig. 2 are calculated using the mathematical algorithm developed elsewhere [18]. As seen due to the short half-life the ^{218}Po activity is negligible at angles $> 100^\circ$ while 7.69 MeV alphas of ^{214}Po could be registered in the whole angular range 0–360°.

In the present measurements α-particles of different radionuclides were separately detected. Aluminum absorbers of three different thicknesses were used for this purpose. The first sector called "A" was shielded with 2.8 mg cm^{-2} absorber. The next "B" sectors were shielded with 6.8 mg cm^{-2} and one sector ("C") was shielded with 11.3 mg cm^{-2}. The range of residual energies of α-particles of ^{218}Po, ^{214}Po and ^{212}Po (^{212}Po is a ^{220}Rn decay product) are shown in Table 1. These energies were calculated using the "range-energy" dependence for Al [19] and considering only alphas with an angle of incidence $\leq 60^\circ$.

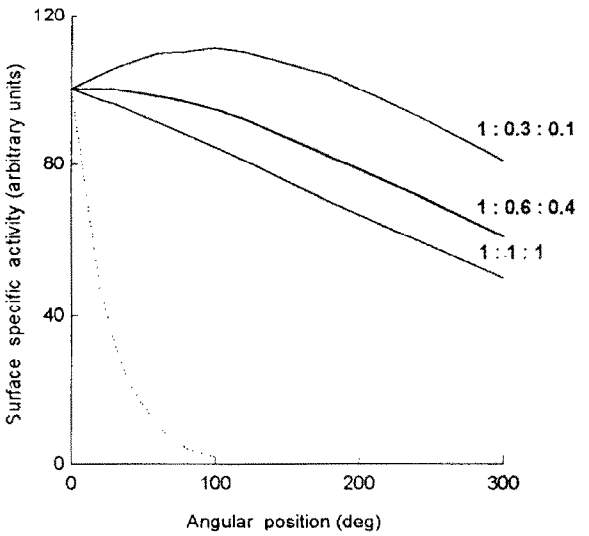

Fig. 2. Theoretical dependencies of the surface specific activities of ^{218}Po (dashed line) and ^{214}Bi + ^{214}Po on the angular position. Assumed activity ratios (^{218}Po:^{214}Pb:^{214}Bi) are shown.

Table 1
Alpha-particle residual energies (in MeV) of ^{218}Po, ^{214}Po and ^{212}Po after transmitting through the absorbers of A-, B- and C-sectors. Incident angles are within the range 0–60°

Sector (Absorber thickness)	Nuclide		
	^{218}Po (6.0 MeV)	^{214}Po (7.69 MeV)	^{212}Po (8.78 MeV)
A (2.8 mg cm^{-2})	2.2–4.4	4.7–6.3	6.1–7.5
B (6.8 mg cm^{-2})	< 0.85	< 3.9	< 5.4
C (11.3 mg cm^{-2})	–	–	< 2.3

As seen from Table 1 ^{218}Po alphas in A-sector fall into the energy window of registration. If present, ^{212}Bi (^{220}Rn decay product) alphas (6.05 and 6.09 MeV) contribute also for tracks in this sector. The energies of ^{212}Po alphas are much higher than the energy window and they are not expected to produce etched tracks in A-sector. It was experimentally obtained that efficiency of registration of ^{214}Po α-particles (7.69 MeV) in A-sector was much lower than that of ^{218}Po alphas. In B-sectors the residual energies of ^{218}Po alphas are insufficient for track formation and only ^{214}Po alphas contribute to tracks from ^{222}Rn progeny. After transmitting through the "C"-absorber only 8.78 MeV alphas of ^{212}Po are of sufficient energy to produce tracks. This sector was used to correct the results for the presence of ^{220}Rn progeny. This correction was necessary because α-particles from ^{212}Bi contribute to tracks in A-sector, respectively, ^{212}Po alphas contribute to tracks in B-sectors.

In the real measurements air sampling continues for a time interval t_a and may vary up to months. After the end of sampling the filter rotation continues until practically all deposited ^{222}Rn and ^{220}Rn short-lived decay products disintegrate (3–4d are sufficient) and after that the SSNTD could be processed. In the present measurements the detector film was etched in 2.5 M NaOH at 60°C for 90 min and the tracks were counted visually by a transmission light microscope. The background was determined in areas located above the clear filter, i.e. away from the trace where radionuclides are deposited.

2.1. Determination of the efficiencies

Consider an absorber-covered SSNTD of a face area S_d which is situated at a small distance from the filter surface where radon progeny atoms are evenly deposited. The "efficiency" of the detector at a sector $p(p = A, B, C)$ to the radiation of the ith radionuclide is defined as follows:

$$\varepsilon_i^{(p)} = \frac{\text{number of tracks}}{\text{number of } i\text{th nuclide disintegrations on the area } S_d}, \quad (1)$$

where $i = 1, 2, 3, 4, 5$ refer to ^{218}Po, ^{214}Pb and ^{214}Bi (+^{214}Po), ^{212}Pb and ^{212}Bi(+^{212}Po), respectively. As SSNTD can register only α-particles then $\varepsilon_2^{(p)} = 0$ and $\varepsilon_4^{(p)} = 0$. Other efficiencies were experimentally determined.

The efficiency $\varepsilon_1^{(A)}$ was determined in the following way: A grab sample of ^{220}Rn progeny was taken with a filter. After a delay time of 6 h, the activities of ^{212}Pb, ^{212}Bi + ^{212}Po and ^{208}Tl were in constant proportions (an equilibrium state). Then a SSNTD (covered with A-absorber) was fixed above the filter and was simultaneously placed on a HPGe detector (∅57.4/44.3 mm, with Model 100U, EG&G ORTEC gamma spectrometer, relative efficiency 24.9%, FWHM(1332 keV) = 1.77 keV). The gamma spectrum was accumulated for a controlled time (24 h). After that the SSNTD was etched and the number of tracks determined. The total number of ^{212}Bi disintegrations was determined by the net area of 727 keV γ-line of ^{212}Bi and 860 keV γ-line of ^{208}Tl. There were two α-emitting ^{220}Rn daughters on the filter. The first one was ^{212}Bi which disintegrates 36% by α-decay [20] emitting α-particles of energies 6.05 and 6.09 MeV. These α-particles are of energies very close to 6.0 MeV of ^{218}Po alphas and were used for the determination of $\varepsilon_1^{(A)}$. The other α-source is ^{212}Po but it could not contribute to tracks in A-sector by reasons stated above. The efficiency $\varepsilon_1^{(A)}$ was obtained by Eq. (1) taking in the denominator the number of the ^{212}Bi α-decays

(i.e. 36% of all ^{212}Bi disintegrations). The result is $\varepsilon_1^{(A)} = 0.097 \pm 0.007$. By analogous measurements with B and C absorbers the values obtained were $\varepsilon_5^{(B)} = 0.023 \pm 0.005$ and $\varepsilon_5^{(C)} = 0.019 \pm 0.002$.

The efficiencies $\varepsilon_3^{(B)}$ and $\varepsilon_3^{(A)}$ were determined as follows: A grab sample of ^{222}Rn progeny was taken with the filter. After a 30 min delay ^{218}Po atoms were essentially disintegrated and the only α-source on the filter was ^{214}Bi + ^{214}Po. Then a SSNTD covered with "A" or "B" type of absorbers was fixed above the filter and the filter + SSNTD were simultaneously placed on a HPGe detector described above. The gamma spectrum was accumulated in 4 h. After that the SSNTD was processed. The total number of ^{214}Bi disintegrations was determined by the net area of 1120 keV γ-line. The results are $\varepsilon_3^{(B)} = 0.087 \pm 0.005$ and $\varepsilon_3^{(A)} = 0.0041 \pm 0.0004$. The obtained value of $\varepsilon_3^{(A)}$ is only about 4% of the $\varepsilon_1^{(A)}$ value, i.e. the present manner of registration could be considered as "spectrometric" regarding ^{218}Po and ^{214}Po alphas.

2.2. Data processing

At first only ^{222}Rn progeny deposited on the filter will be considered. According to the mathematical algorithm developed elsewhere [18] the track net-number (i.e. background subtracted) in the kth sector whose center is placed at an angle φ_k is given by the expression:

$$C_k = C(\varphi_k) = \sum_{i=1}^{3} F_i(\varphi_k) X_i. \tag{2}$$

The relationship between the parameters X_1, X_2 and X_3 and the integrated volume specific activities is linear:

$$I_i = \int_0^{t_a} A_{ri}(t)\,dt = \sum_{j=1}^{3} R_{ij} X_j, \tag{3}$$

The expressions for the matrix R_{ij} and $F_i(\varphi)$ functions are derived in another paper Ref. [18]. Their explicit forms used in the calculations are

$$R_{ij} = \frac{1}{V\eta\varepsilon_3^{(B)}} \begin{pmatrix} \dfrac{\lambda_1(\lambda_1-\lambda_2)(\lambda_1-\lambda_3)}{\lambda_2\lambda_3} & 0 & 0 \\ -\dfrac{\lambda_1(\lambda_1-\lambda_3)}{\lambda_3} & -\dfrac{\lambda_2(\lambda_2-\lambda_3)}{\lambda_3} & 0 \\ \lambda_1 & \lambda_2 & \lambda_3 \end{pmatrix}, \tag{4}$$

$$F_i(\varphi_k) = \left\{ \left[\frac{2h\omega r_c}{\lambda_i} \operatorname{sh}(\lambda_i \Delta\varphi_k/\omega) \right] \times \frac{\exp(\lambda_i t_F) - 1}{1 - \exp(-2\pi\lambda_i/\omega)} \exp(-\lambda_i \varphi_k/\omega) \right\} \times \left\{ 1 + \delta_{k1} \left[\varepsilon_3^{(A)}/\varepsilon_3^{(B)} + \frac{(\lambda_1-\lambda_2)(\lambda_1-\lambda_3)\varepsilon_1^{(A)}}{\lambda_2\lambda_3\varepsilon_3^{(B)}} \delta_{i1} - 1 \right] \right\}, \tag{5}$$

where V is the air velocity through the filter (V = air flow rate/nozzle inlet area), η is the filter efficiency, δ_{ik} is the Kronecker symbol ($\delta_{ik} = 1$ if $i = k$ and 0 if $i \neq k$), λ_i are the decay constants, h is the height of the sector, r_c is the radius of the circle passing through the sector centers, t_F is the time for which a given point of the rotating filter passes through the inlet nozzle, ω is the angular velocity of the rotating filter. The indices $i = 1, 2, 3$ in λ_i, I_i and A_{ri} refer to ^{218}Po, ^{214}Pb and ^{214}Bi, respectively. The X_i parameters were estimated by the least-squares fit of the experimentally determined number of tracks in different sectors – through minimization of the form

$$\sum_{k=1}^{n} \left[C_k - \sum_{i=1}^{3} F_i(\varphi_k) X_i \right]^2. \tag{6}$$

Uncertainties σ_i in I_i were calculated as follows:

$$\sigma_i = \left[\sum_{k=1}^{3} \sum_{l=1}^{3} R_{ik} R_{il} \operatorname{Cov}(X_k, X_l) \right]^{1/2}, \tag{7}$$

where the covariation $\operatorname{Cov}(X_k, X_l)$ is given by the expression:

$$\operatorname{Cov}(X_k, X_l) = \frac{\sum_{p=1}^{n} [C_p - \sum_{i=1}^{3} F_i(\varphi_p)\hat{X}_i]^2}{n-3} (K^{-1})_{kl}. \tag{8}$$

In Eq. (8) K^{-1} is the inverse matrix of the matrix with elements $K_{ij} = \sum_k F_i(\varphi_k) F_j(\varphi_k)$ and $\hat{X}_i$ are the least-squares estimates of X_i.

All calculations were performed by a software based on the algorithm described.

2.3. Optimization of the design

As indicated by our experience the experimental uncertainties are significantly dependent on the choice and disposition of the different sectors, their number, etc. In order to ensure the maximum accuracy of the measurements, numerical experiments were made. Their purpose was to study the propagation of uncertainties on variation in different parameters. In these numerical experiments the statistical uncertainty was ascribed to the track counting and a Poisson distribution of number of tracks was assumed.

First, the disposition of the A-sector was chosen. The starting angle for this sector was 2°. The uncertainties in ^{218}Po, ^{214}Pb and ^{214}Bi were studied as dependent on the width of this sector. The B-sectors start immediately after the A-sector and every B-sector is of 20° angular width. The results showed that the uncertainty in ^{218}Po was decreasing for wider A-sector, but the uncertainty in ^{214}Bi was increasing. The uncertainty in ^{214}Pb was weakly dependent on this parameter. As optimal width has been considered that, for which the sum $\sigma_1^2 + \sigma_2^2 + \sigma_3^2$ is a minimum. As seen in Fig. 3 the optimal width is

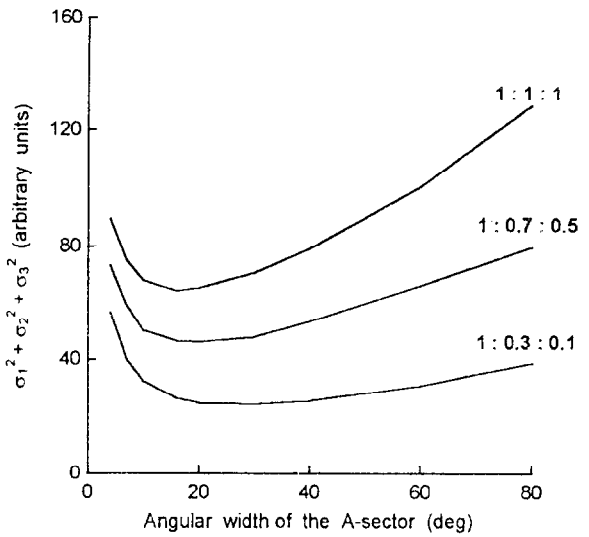

Fig. 3. Dependence of $\sigma_1^2 + \sigma_2^2 + \sigma_3^2$ on the angular width of the A-sector. Assumed activity ratios (^{218}Po:^{214}Pb:^{214}Bi) are shown.

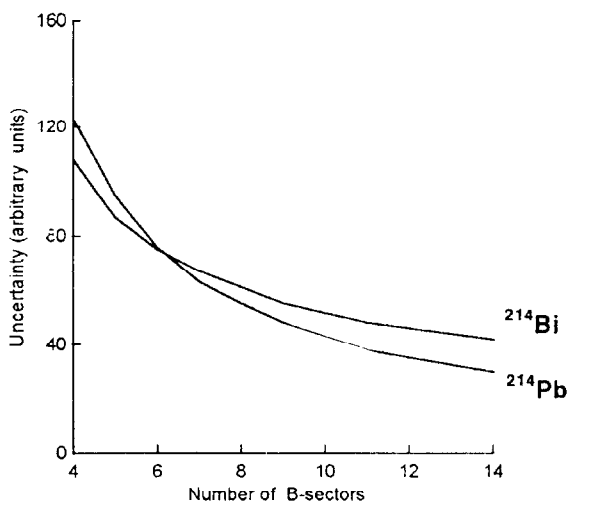

Fig. 4. Uncertainties of ^{214}Pb and ^{214}Bi as dependent on the number of B-sectors.

about 20° for a great variety of activity ratios ^{218}Po:^{214}Pb:^{214}Bi. This was convenient for the practice as all sectors of SSNTD film in the present measurements were of one and the same angular width of 20° and of equal areas.

The dependence of uncertainties in ^{214}Pb and ^{214}Bi on the number of B-sectors is shown in Fig. 4. As seen if the number of sectors is small (e.g. less than 8) the uncertainties grow rapidly. In the present experiments the number of sectors used was ≥ 8.

2.4. Correction for ^{220}Rn-progeny availability

If short-lived ^{220}Rn progeny are present in measurable concentrations they could affect the results both for A- and B-sectors. However, the correction of ^{220}Rn progeny is much facilitated by the following reason: For the fixed period of rotation (1 h) the angular dependence of the surface specific activity of ^{212}Bi + ^{212}Po (both directly deposited and produced by the ^{212}Pb decay) is weak. For activity ratios ^{212}Bi:^{212}Pb ≤ 1 (the real case, according to the published results [21]) the angular variation of the specific activity (max–min) is from 7% (^{212}Bi = ^{212}Pb) to less than 2% (^{212}Pb $\gg$ ^{212}Bi). If this activity is considered as constant for all angular positions and corresponding to the value of sector C (situate with center at 192°, width 20°), the deviation of the real surface specific activity will not exceed $\pm$ 4% of this value. This difference is sufficiently less than the normal experimental uncertainties in our experiments.

Experimentally, this correction was made as follows: The net-number of tracks in the sector C was C_T, hence the number of ^{212}Bi disintegrations in this sector was $C_T/\varepsilon_5^{(C)}$. Taking this number as a constant for all sectors the expected number of tracks in the A-sector due to the ^{220}Rn progeny on the filter were: $0.36\, C_T \varepsilon_1^{(A)}/\varepsilon_5^{(C)}$ and for B-sector (affected by 8.78 MeV α-particles): $C_T \varepsilon_5^{(B)}/\varepsilon_5^{(C)}$. Note that 0.36 is the probability of ^{212}Bi α-decay. These values were subtracted from the total number of the tracks in the correspondent sectors.

The net-number of C-sector tracks could also be used for assessment of the time-integrated PAEC of ^{220}Rn progeny. The theoretical analysis showed that integrated PAEC (^{220}Rn) is proportional to C_T with less than 1% variation due to the differences in ^{212}Pb:^{212}Bi ratio. More details about integrated measurements of ^{212}Pb and ^{212}Bi in air are described elsewhere [22].

3. Results and discussion

Measurements following the present method have been made in an experimental basement where ^{222}Rn-progeny concentrations varied within the range of 15–200 Bq m^{-3} and concentrations of ^{220}Rn progeny were from < 0.5 to about 3.5 Bq m^{-3}. The average ratio PAEC(^{220}Rn):PAEC(^{222}Rn) was about 0.4. Thus, the situation in this basement was similar to the situation in dwellings where both ^{222}Rn and ^{220}Rn are present [23]. Some measurements were performed at the National Center of Metrology (Bulgaria) in an artificial ^{222}Rn atmosphere free from ^{220}Rn progeny. All measurements were made at an air flow-rate of 1.2 l min^{-1}. During these tests reference measurements were made made with the method of Kritidis et al. [7].

Results from such comparative measurements are shows in Table 2. They cover the range of integrated

Table 2
Integrated concentrations following the present method compared with simultaneously made series of grab-sampling measurements. The results are given in Bq h m^{-3}

Present method ^{218}Po	^{214}Pb	^{214}Bi	Grab samplings ^{218}Po	^{214}Pb	^{214}Bi
870 ± 150	930 ± 120	700 ± 140	830 ± 100	770 ± 25	590 ± 32
249 ± 21	101 ± 26	72 ± 20	234 ± 39	119 ± 9	60 ± 12
599 ± 72	369 ± 54	280 ± 60	554 ± 168	381 ± 55	329 ± 34
196 ± 16	62 ± 14	52 ± 15	159 ± 79	40 ± 20	20 ± 15
530 ± 40	446 ± 29	336 ± 40	659 ± 90	466 ± 60	390 ± 39
4500 ± 250	1410 ± 110	490 ± 70	5050 ± 460	1760 ± 190	570 ± 130

concentrations from about 20 to about 5000 Bq h m^{-3}. The ^{218}Po : ^{214}Pb : ^{214}Bi activity ratios varied from a disequilibrium of 1 : 0.3 : 0.1 to about a full equilibrium. The agreement between the results by the present method and the reference values is clear. The experimental uncertainties were individual for any measurement, but their relative values were $\leq 20\%$ for most of the integrated concentrations above 100 Bq h m^{-3}. Note that a quantitative agreement was obtained for low-integrated concentrations – even less than 100 Bq h m^{-3}. At typical environmental conditions 100 Bq h m^{-3} refer to a time of sampling of few hours indoors and about 1 d outdoors. Thus, the method is expected to cover the practical range of concentrations for the measurements in the human environment. In high concentrations the method is limited by the SSNTD saturation. At an air flow rate of 1.2 l min^{-1} saturation is expected to occur above 5×10^5 Bq h m^{-3}. This limit could be made higher reducing the air flow-rate through the rotating filter. However, if this reduction is significant new test measurements should be performed in order to check if problems due to the plateout losses of ^{222}Rn progeny have arisen.

3.1. Spectrometric versus non-spectrometric version of the method

In principle, the manner of registration of α-particles by SSNTD could be arranged "non-spectrometrically", for instance, using SSNTD with wider energy range of sensitivity (e.g. CR-39) so that the use of absorbers will not be necessary. Measurements with a non-spectrometric approach have not been made but the uncertainties were studied by numerical experiments. At one and the same integrated concentrations where the α-particle efficiency of the non-spectrometric method was 0.1 the relative uncertainties in ^{218}Po, ^{214}Pb and ^{214}Bi were, respectively, 4, 1.2 and 1.7 times greater for the non-spectrometric than for the spectrometric method. The accuracy of the spectrometric method for ^{218}Po could not be competed by the non-spectrometric one even if the latter operates with the maximum possible efficiency of 0.5.

4. Conclusions

A method for integrated measurements of individual concentrations of each of the short-lived ^{222}Rn progeny (^{218}Po, ^{214}Pb and ^{214}Bi + ^{214}Po) has been proposed. It is based on a combination of the rotating filter and SSNTD shielded with absorbers. The experimental results obtained suggest that the method is adequate at integrated concentrations as low as 100 Bq h m^{-3}. Therefore, the sensitivity of the method is sufficient for measurements of ^{222}Rn progeny in the range of concentrations which are typical in the human environment.

Acknowledgements

This work was partly supported by the Committee on the Use of Atomic Energy for Peaceful Purposes (Bulgaria) under contracts 61-92 and 159-96. I am grateful to Tanya Boshkova for the help in gamma spectrometry measurements and to T. Semova and A. Proykova for the help in preparing the manuscript.

References

[1] W.F. Bale, US-AEC (1951) unpublished memorandum; reprinted in Health Phys. 38 (1980) 1061.
[2] UNSCEAR 1993 Report to the General Assembly, UN Publications, New York, 1993.
[3] A.C. George, Health Phys. 70 (1996) 451.
[4] E.C. Tsivoglou, H.E. Ayer, D.A. Holaday, Nucleonics 11 (1953) 40.
[5] O.G. Raabe, M.E. Wrenn, Health Phys. 17 (1969) 593.
[6] J.W. Thomas, Health Phys. 23 (1972) 783.
[7] P. Kritidis, I. Uzunov, L. Minev, Nucl. Instr. and Meth. 143 (1977) 299.
[8] R.J. Trembley, A. Leclerc, C. Mathieu, R. Pepin, M.G. Townsend, Health Phys. 36 (1979) 401.
[9] D.S. Pressyanov, M.G. Gelev, O.J. Penchev, US Patent 5,225,673 priority date, 4 January 1991.

[10] J.P. McLaughlin, B. Fitzgerald, Rad. Prot. Dosim. 45 (1992) 115.
[11] D.S. Pressyanov, M.G. Guelev, O.J. Pentchev, Health Phys. 64 (1993) 522.
[12] Annals of the ICRP 23,2 1993, ICRP Publication 65.
[13] R.L. Grasty, Health Phys. 66 (1994) 185.
[14] J.G. Price et al., Health Phys. 66 (1994) 433.
[15] D.S. Pressyanov, M.G. Guelev, B.G. Sharkov, Atmos. Environ. 29 (1995) 3433.
[16] D.S. Pressyanov, M.G. Guelev, O.J. Pentchev, P.P. Kritidis, Environ. Int. 22 (1996) S607.
[17] R. Barillon, Ph.D. Thesis, University Franche-Comte, 1994 (in French).
[18] D.S. Pressyanov, Nucl. Instr. and Meth. A 397 (1997) 455.
[19] V.P. Mashkovitch, Protection Against Ionizing Radiation, Handbook, Energoatomizdat, Moscow 1982 (in Russian).
[20] C.M. Lederer, V.S. Shirley (Eds.), Table of Isotopes, 7th ed., Wiley, New York, 1978.
[21] A. Reineking, G. Butterweck, J. Kesten, J. Porstendorfer, Rad. Prot. Dosim. 45 (1992) 353.
[22] D.S. Pressyanov, Health Phys. 68 (1995) 261.
[23] R.W. Sheets, Radioact. Radiochem. 4, 1 (1993) 46.